ORIGINAL ARTICLE

Development of Microstructure Homogeneity and Mechanical Properties After ECA-Extrusion of Copper Alloy C11000

Behzad Tolaminejad[1] · N. Fakhar[2]

Abstract The C11000 billets were intensely deformed through equal channel angular extrusion (ECAE) up to eight passes. The deformed microstructure of the billet was assessed by electron-backscattered diffraction (EBSD). The mechanical properties of the extruded billets were evaluated by tensile and hardness tests. The microhardness and microstructural investigations at different positions of the billet thickness revealed development and homogeneity by increasing the number of passes. This result was approved by the uniform distribution of effective strain in the ECA-extruded samples at high passes which was obtained by DEFORM-3D software. It became clear that the average microhardness is significantly raised up to four passes of ECAE and thereafter it is slightly reduced when more passes are applied. Utilizing the sub-structural data, the yield strength of the billets was predicted. The model is consistent with the experimental results.

Keywords Equal channel angular extrusion · Ultrafine grain · Strength · C11000 alloy · Homogeneity

1 Introduction

Copper alloys are commonly utilized as electrical and thermal interface materials due to their attractive conductivity, resistant to corrosion as well as good strength and ductility [1, 2]. Ultrafine-grained (UFG) materials have been conspicuous in recent years arising from the unusual properties of these materials [3, 4]. Severe plastic deformation (SPD) processes are widely used for the production of UFG structures and obtaining moderately large bulk samples without residual porosity [5]. The most familiar process of SPD is the equal channel angular pressing or extrusion (ECAE) which has been extensively applied on the diverse range of metals [5–7]. This process consists of extrusion of a billet through two channels, intersecting at the inner and outer corner angles Φ and Ψ, having the same cross section. Equation (1) describes the equivalent strain up to N passes [8]:

$$\overline{\varepsilon}_N = \frac{N}{\sqrt{3}}\left[2\cot\left(\frac{\Phi+\Psi}{2}\right) + \psi\cos ec\left(\frac{\Phi+\Psi}{2}\right)\right] \quad (1)$$

Under ideal conditions, it has been confirmed that a sample extruded through an ECAE die undergoes a homogeneous simple shear strain, whereas it should be noted that the strain during ECAE is not actually homogeneous [9]. In spite of the several publications clarifying the tailored microstructures, through-thickness microstructure gradients after subsequent passes of ECAE have been slightly investigated. For instance, Terhune et al. [10] examined solely the top of the billet for microstructural analysis and recommended the homogeneities after a small pass numbers. Necker et al. [11] explained that consecutive passes based on route B_C did not homogenize the strain in the samples. However, in two other reports, it was noted that the homogeneity increased after eight passes [12, 13]. Regarding the restricted and conflicting area of these researches, in this investigation it is attempted to evaluate the through thickness homogeneity of the ECA-extruded samples via microstructural observations, microhardness variations and effective strain distribution. Utilizing the structural parameters–flow stress correlation,

✉ Behzad Tolaminejad
  tolaminejad@hut.ac.ir

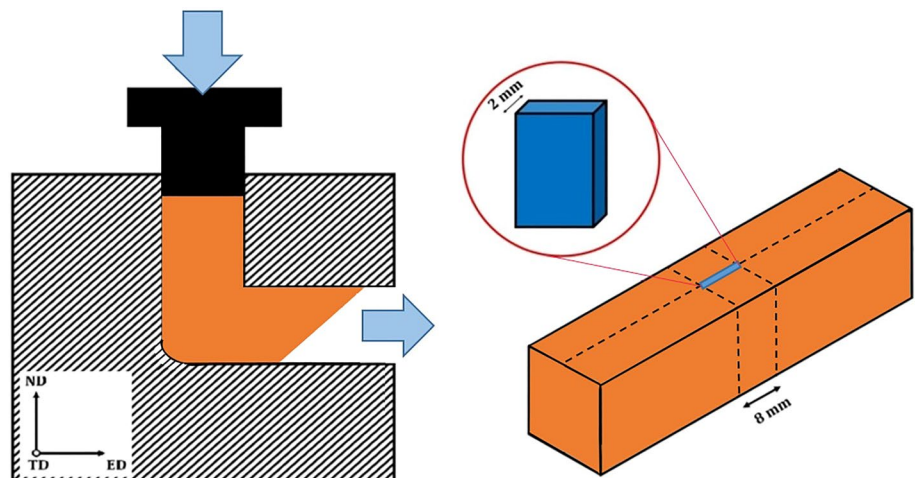[1] Department of Materials Science and Engineering, Hamedan University of Technology, Hamedan, Iran

[2] Department of Mechanical Engineering, Hamedan University of Technology, Hamedan, Iran

the yield strength was predicted and compared with measured values.

2 Experimental Procedure

The material utilized in this research consisted of copper alloy UNS C11000 (99.95%). The dimensions of copper billet were $70 \times 14 \times 14$ mm. The ECAE process was executed at ambient temperature using a die with an inner angle of $\Phi = 90°$ and outer angle of $\Psi = 20°$. Samples were extruded up to 8 passes through route B_C (rotation by 90° after every pass). To evaluate the microstructure, specimens with dimensions of $14 \times 7 \times 2$ mm (normal direction (ND) $\times$ extrusion direction (ED) $\times$ transverse direction (TD), respectively) were cut from the ECAE-ed copper (Fig. 1). The microhardness evaluation was repeatedly performed through the thickness using a MHT-1 tester equipped with a Vickers indenter under a load of 200 g for a time of 20 s. These points were described by a parameter S, which defines $\Delta t / t_0$, where Δt and t_0 are the distance of the examined positions from the bottom surface in the central regions and sample thickness, respectively. The tensile test specimens were prepared from the as-extruded materials (ASTM E-8), and uniaxial testing was carried out using an Instron 5582 universal tester at a constant strain rate equal to 10^{-3} s^{-1}. For EBSD orientation mapping, the surfaces were electro-polished in a solution composed of 2:3 H_2O/H_2PO_4 (85 vol.%) at -20 °C and a voltage of 45 V. The EBSD characterization was performed by means of TSL OIM data collection 7 in Philips XL-30 FEG SEM worked at 15 kV. The copper specimens were studied in three different depths: $S = 0.1$ (i.e., 1.5 mm from the bottom), $S = 0.5$ and $S = 0.9$. For each depth, some orientation maps were considered using an 80-nm step size on the overall area of approximately 80 μm $\times$ 20 μm.

3 Finite Element Modeling

ECAE process of copper billets was simulated with the help of Deform 3D software up to 8 passes. The die and ram were modeled as a rigid body, whereas the sample was simulated as an elastic–plastic material. The die geometry, sample size and ram speed were the same as the experiments. The material behavior of the copper was achieved from the tensile tests. The stress–strain curves of the as-received copper and the deformed billets after different passes of ECAE are plotted in Fig. 2. The specimen was meshed using 30,000 elements. The automatic remeshing was implemented if the elements became too distorted through simulations. In order to evaluate the homogeneity of the process, the distribution of strain accumulated in the sample after 1, 4 and 8 passes was studied. The strain inhomogeneity index (ε^*) was also determined by the equation given below [14]:

$$\varepsilon * = \left(\varepsilon_{p(\max)} - \varepsilon_{p(\min)} \right) \Big/ \varepsilon_{p(avg)} \tag{2}$$
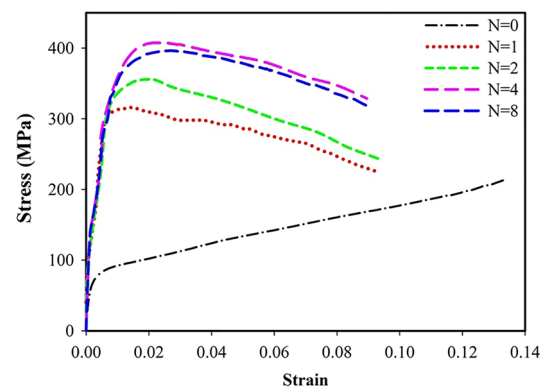
Fig. 2 Tensile stress–strain curves for C11000 copper at room temperature after different ECAE passes

Fig. 1 Schematic feature of the coordinate and specimen based on the ECAE die

where $\varepsilon_{p(max)}$, $\varepsilon_{p(min)}$ and $\varepsilon_{p(avg)}$ are the maximum, minimum and average effective plastic strains, respectively.

4 Results and Discussion

The average grain size of the undeformed copper billet was estimated as 34 μm (Fig. 3). Figure 4 illustrates the orientation color maps taken from several positions in the Cu sample after one ECAE pass. The majority of the microstructure in the middle (S = 0.5) and top (S = 0.9) consists of some elongated (sub) grains. The fibrous structures might have caused by the continued subdivision of some deformation bands (DBs) [15]. The extension of the microstructures at S = 0.5 is around 45°. It is clear that in ECAE under ideal circumstances, the mode of process is simple shear [16]. However, at S = 0.9, subgrains are matched with an angle which is smaller than 45° but nearly similar to that of S = 0.5 (Fig. 4a, b). This may be attributed to the friction between the sample and the die bringing in an additional

shear. Besides, this shear may raise the considerable strain beyond the strain applied in the ECAE. Hence, it is anticipated that at S = 0.9, the microstructural development takes place more rapidly than near S = 0.5 middle position. These results are in agreement with the FEM research described by Kim et al., proving a larger equivalent strain in the vicinity of top surface of ECAE sample [17]. While, the microstructure at the bottom (S = 0.1) indicates larger and more equiaxed grains, similar to the initial microstructure (Fig. 4c). Under this condition, the effect of friction may be ignored due to a small gap between the billet and the die wall during deformation in spite of the outer corner angle [18]. The calculated orientation distribution functions (ODFs) of this specimen (in Bunge's notation) shown in Fig. 5 justify the nature of the microstructural refinement and morphology at different positions. The FCC shear textures have been categorized into three components: A {111} < hkl >, B {hkl} < 110 > and C {001} < 110 >. These orientations are of two incomplete fibers: {111}$_\theta$ < uvw > with a {111} plane counter clockwise rotated by θ about TD from the ND and {hkl} < 110 >$_\theta$ with a < 110 > direction revolved. ODF plots can separate some components, such as A$_\theta$, Ā$_\theta$, A*$_{1\theta}$, which partly overlap in the pole figures [19]. The position of the ideal shear components in the ODF section is shown in the key figure. The ODF sections of S = 0.1 (Fig. 5a) exhibit a major texture component that is cube. This component is generally accepted as deformation and recrystallization texture component distinguished in Cu alloys. Indeed, the starting texture has a significant effect on texture development during ECAE [20], since the strain through each pass is not enough to extinguish the texture prehistory. At S = 0.5, the φ$_2$ = 0° Sect. (0° < φ$_1$ < 180°; 0° < φ < 90°) shows A$_{1\theta}$ and C$_\theta$ components in addition to a stronger but wide spread A$_{2\theta}$ components. A relatively larger spread has been identified around the ideal location of A$_\theta$ and B$_\theta$/B̄$_\theta$ components. Meanwhile, continuous orientation distribution joining A$_\theta$, B$_\theta$ and C$_\theta$ components (B fiber) in the ODF is observed. The absolute intensities of these components are non-uniform.
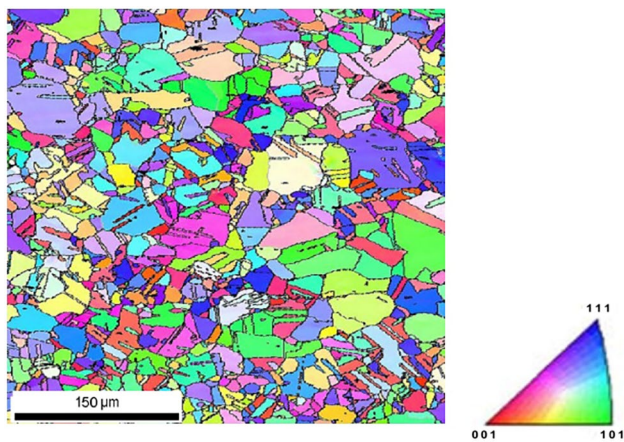
Fig. 3 EBSD color map illustrating the microstructure of the initial undeformed specimen
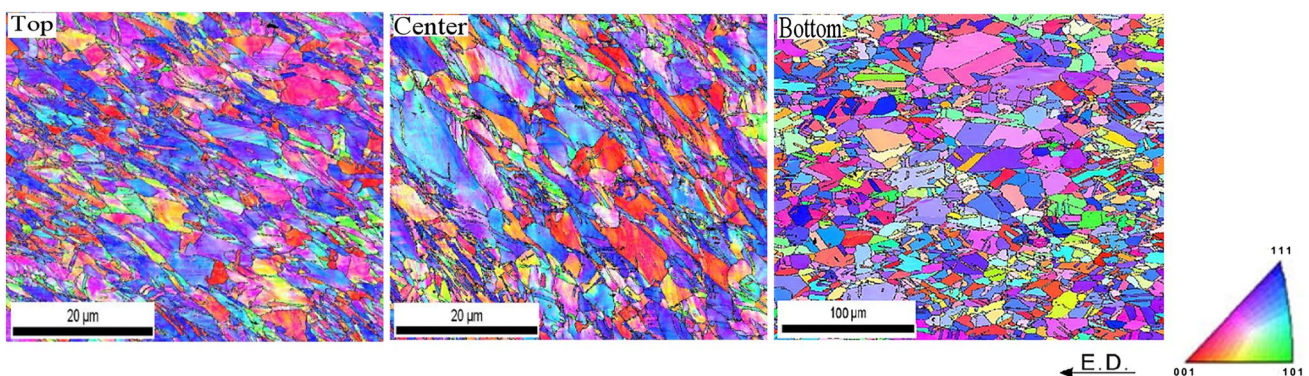
Fig. 4 The EBSD orientation color maps achieved from different positions of the specimen experienced 1-pass ECAE
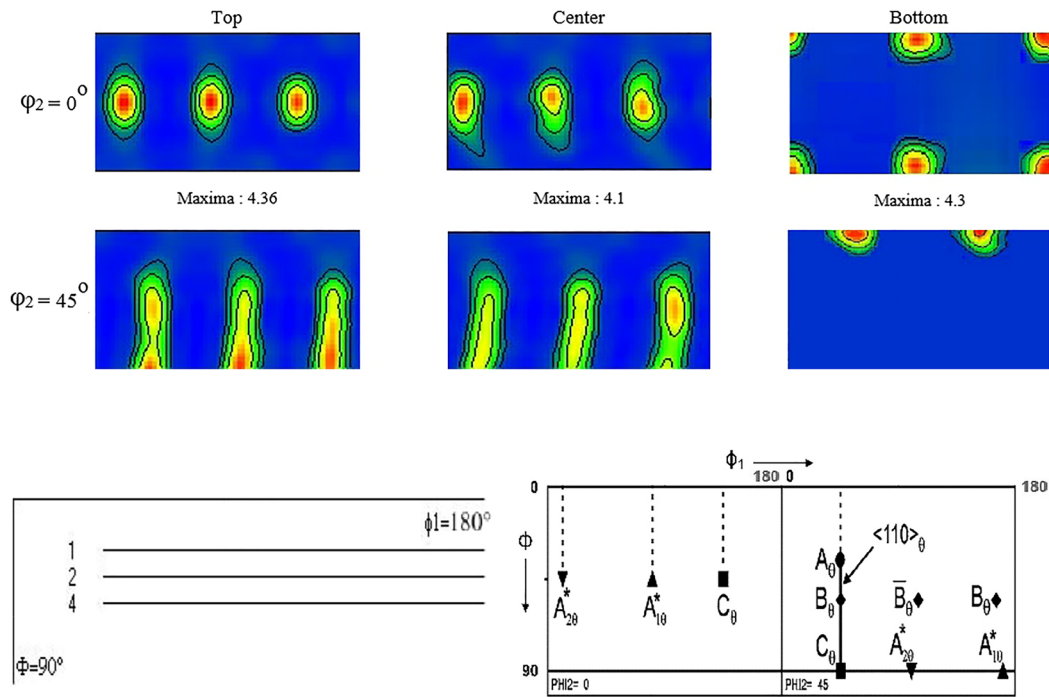
Fig. 5 $\varphi_2 = 0°$ and $\varphi_2 = 45°$ ODF sections of textures measured from different positions after 1-pass ECAE accompanied by the key figure showing ideal orientations [23]

Similar connection between the components $\overline{B}_\theta$, $A_{2\theta}$ and B_θ, $A_{1\theta}$ could be noticed because of the strong intensity of $\overline{B}_\theta$ component. It is clear that the texture at $S = 0.9$ looks very similar to that of $S = 0.5$. But, the B fiber shrinks to its B_θ component. Also, the intensity of the $A*_1$, $A*_2$ and C components increases toward the top surface. The substitute deformation systems of type $A*_1$ and $A*_2$ could have been developed by the block of the dislocation mobility because of the extensive subgrains generated [21].

Color maps acquired in different sections of the samples after 4- and 8-pass of ECAE are demonstrated in Figs. 6 and 7. From Fig. 6, the prior texture is evolved mainly to (101)

and (111) to (100) at middle ($S = 0.5$) and top ($S = 0.9$), respectively, while the texture of the bottom surface ($S = 0.1$) is different to some extent according to the standard stereographic triangle; hence, the through thickness texture is inhomogeneous even after four passes. The large elongated microstructures related to one pass are fragmented into equiaxed or small elongated grains. The heterogeneity of the microstructure through the sections is in contrast to that reported for aluminium [22]. This is probably due to the fact that the uniform microstructure with either high or low SFE is rather attained than that of metals with intermediate value of SFE during ECAE [23]. Also, the work hardening
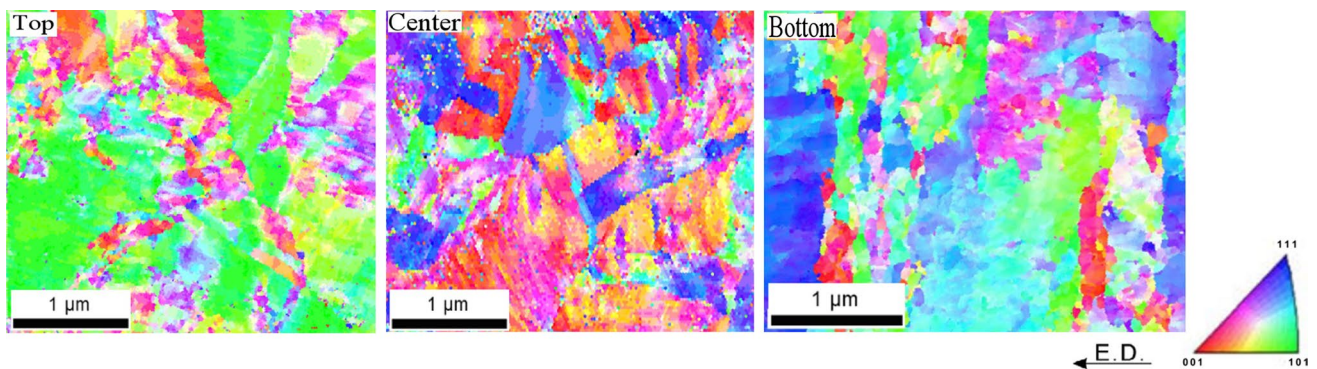
Fig. 6 The EBSD orientation color maps achieved from various positions of the specimen experienced 4-pass ECAE
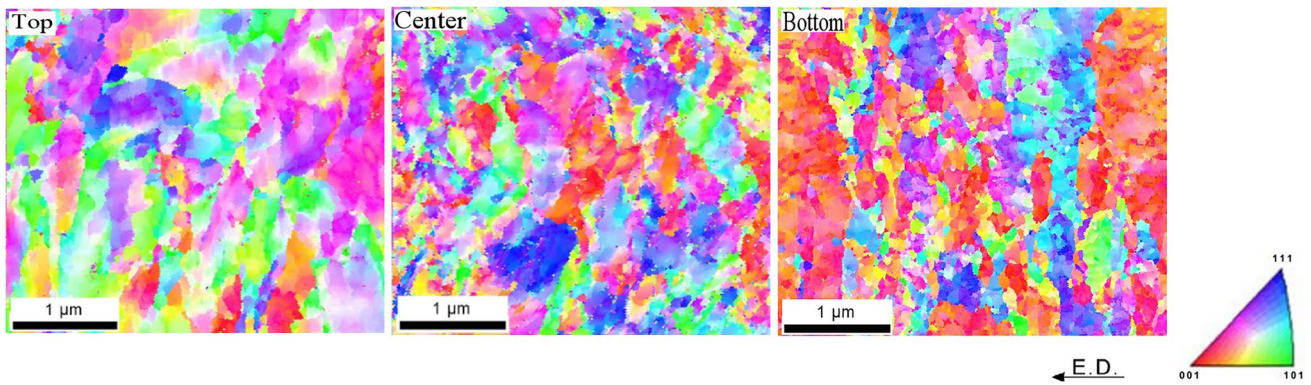
Fig. 7 The EBSD orientation color maps achieved from different positions of the specimen subjected to 8-pass ECAE

of the material should be taken into account [9]. On the other hand, the microstructure of specimen after 8-pass is more homogeneous than that of previous specimens in the light of grain morphology. Moreover, the microstructure mainly consists of uniform texture and an equiaxed microstructure of a finer grain size is obtained (Fig. 7).

The distributions of the misorientation angles are shown in Fig. 8 for the specimens extruded through 4 and 8 passes. Although the fraction of high-angle grain boundaries (HAGBs: misorientation > 15°) increases to 69.6%, some low-angle boundaries (LAGBs) have already appeared after 4th pass and the average misorientation angle is 28.7°. During the subsequent deformation (up to 8 passes), the average fraction of HAGBs and misorientation angle increase significantly to 81.4% and 35.7°, respectively. Indeed, the majority of the microstructure contains HAGBs. By rising passes of ECAE, dislocation's mobility inside the grains may become harder due to the prevention of the intergranular strains. The plastic deformation could be adapted by (sub) grain rotation, which promotes the enhancement of HAGBs fraction and the generation of new finer grains [24]. Also, the distribution of misorientation angles at S = 0.5 shows the peaks (Fig. 8b). The bimodal distribution is a feature of severely deformed materials [25]. Grains not oriented in any stable orientation following the subjected strain field will be subdivided by DBs rotating into stable orientations. Deformation banding
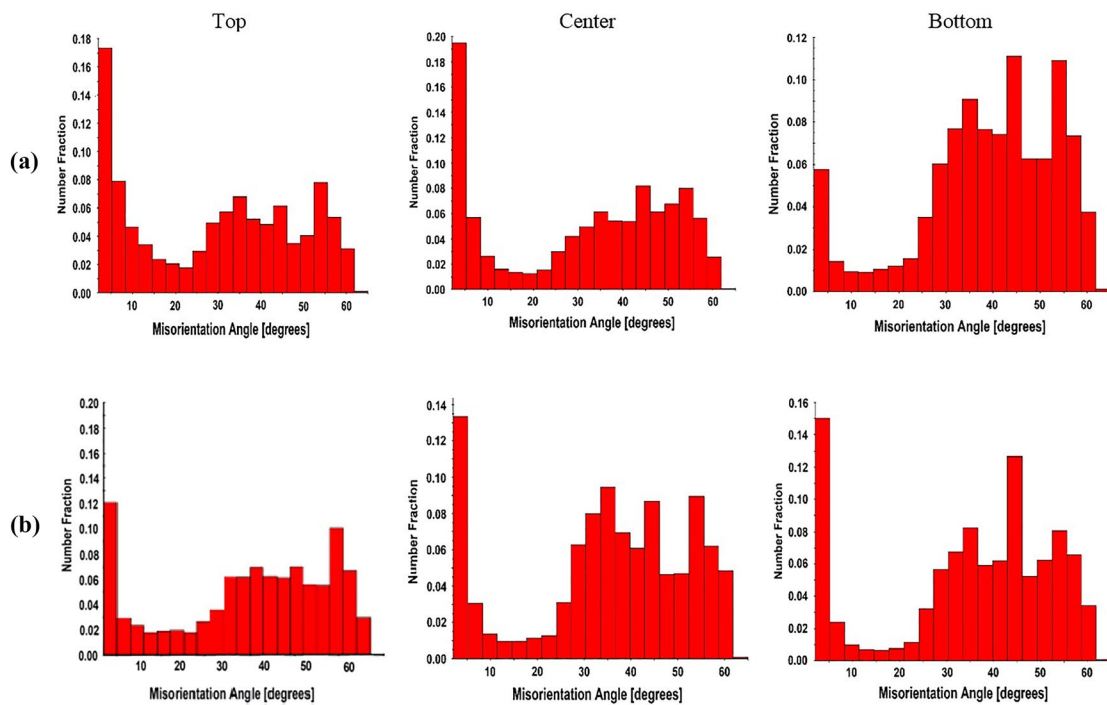
Fig. 8 Distribution of the grain boundaries misorientation angle at the center, top and bottom of the specimens after **a** 4 passes and **b** 8 passes

has two probable sources. Based on the first theory [26], these bands initiate as a result of the ambiguity in selection of the operative slip systems. Another source is given by inhomogeneous straining, i.e., various regions of a grain may experience different strains. The DBs are subdivided by geometrically necessary boundaries (GNBs). Moreover, boundaries are also created by statistical trapping of dislocations, so-called incidental dislocation boundaries (IDBs). It is worth mentioning that the misorientation of both items principally rises with strains [27].

Figure 9 shows the microhardness data versus normalized distance from bottom of the billet. These results are illustrated after several passes, and the lower solid points represent determined data in the as-received state. The single-pass ECAE evidently creates an inhomogeneous hardness distribution at S = 0.1 where the hardness value is notably smaller than in the other sites. Likewise, there are larger error bars after first pass as a result of higher inhomogeneity. On the contrary, the inhomogeneity decreases after 4th pass in terms of reduction in the extent of the error bars and the points of low hardness close to the bottom (S = 0.1). The hardness declines to some extent after 8th pass, and the degree of homogeneity is developed beyond 4th pass. The mean value of the hardness has been considered for all the samples. Contour plots of effective strain distribution and their related histograms up to 8 passes of ECAE are demonstrated in Fig. 10. It is clear that by increasing the number of passes, the accumulated strain increases. Based on the theoretical calculations, after 4 passes the average of strain would be 4 and as it is seen in Fig. 10b, most of the elements experience such a strain. The histograms show that by increasing the number of passes, the percentage of elements which have the same amount of strain is increasing. After 8 ECAE passes, nearly 50% of elements have the strain
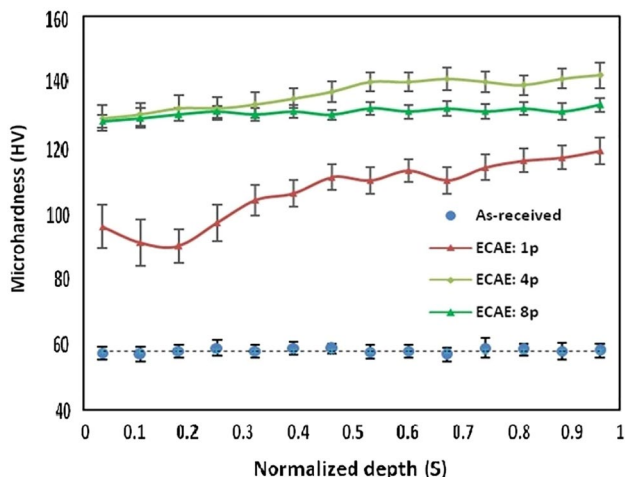

Fig. 9 Values of the Vickers microhardness on the flow plane after ECAE through 1, 4 and 8 passes

of about 7.5. It can be concluded that more deformation homogeneity is achieved at higher passes (Fig. 10c).

A deformed sample can be separated into three deformation zones along the extrusion direction (Fig. 11a). The deformation heterogeneity with non-uniform effective strain distribution is shown in head of deformation zone (HDZ). Also, the tail deformation zone (TDZ) is not a wholly deformed area with deformation heterogeneity, while the main deformation zone (MDZ) occupies the most area with the best homogeneity. The actual trend of strain enhancement across the XY path after 1, 4 and 8 passes is obvious in Fig. 11b. After first pass, the amount of strain increases by approximately 250% in bottom-side-up. This large strain increment illustrates the non-uniformity of the deformed sample. For two other ECA-extruded specimen, the maximum strain enhancement during the path is about 50% and it remains almost constant in the middle part of the thickness. Hence, it can be concluded that after 4 and 8 passes, there is a reasonable degree of uniformity in the deformed specimen. The same trend of strain distribution for different ECAE passes in the thickness direction was reported earlier [14, 28]. To evaluate the degree of homogeneity, the strain and microhardness distribution through thickness were compared for different ECAE passes by calculating the inhomogeneity index of strain (ε^*) and the hardness (H^*):

$$H* = \left(HV_{max} - HV_{min} \right) / HV_{avg}; \quad \varepsilon* = \left(\varepsilon_{max} - \varepsilon_{min} \right) / \varepsilon_{avg} \tag{3}$$

These indices are plotted in Fig. 11c. It can be observed that both the H^* and ε^* are decreasing with increasing the number of passes. In this figure, a relatively sharp reduction from one to fourth pass is followed by a slow reduction from 4- to 8-pass ECAE process. Thereby, the obtained homogeneity in the microstructure and microhardness are consistent with the FEM simulations.

Figure 12 exhibits the yield strength versus the number of passes. Additionally, the average value of the hardness data is plotted. There are two types of boundaries in deformed pure FCC materials of medium to high SFE [29]. First, IDBs which have low-angle misorientations and their strengthening are via dislocations. Second, GNBs contribute to strength through grain boundary mechanism [30]. Accordingly, the yield strength is determined by a combination of these mechanisms as follows [31, 32]:

$$\sigma = \frac{2G}{1-\upsilon} e^{\frac{-2\pi h}{b(1-\upsilon)}} + \left[MG\alpha\sqrt{3b\theta_{LAB}(1-f)} + k\sqrt{f} \right] d^{-1/2} \tag{4}$$

The first term is used to describe the Peierls–Nabarro (friction) stress. Here G, υ, h and b are the shear modulus, Poisson's ratio, primary slip step and Burger's vector, respectively. On the other hand, M is the Taylor factor, α is

Fig. 10 Contour plots of effective strain distribution after **a** 1, **b** 4 and **c** 8 passes of ECAE process
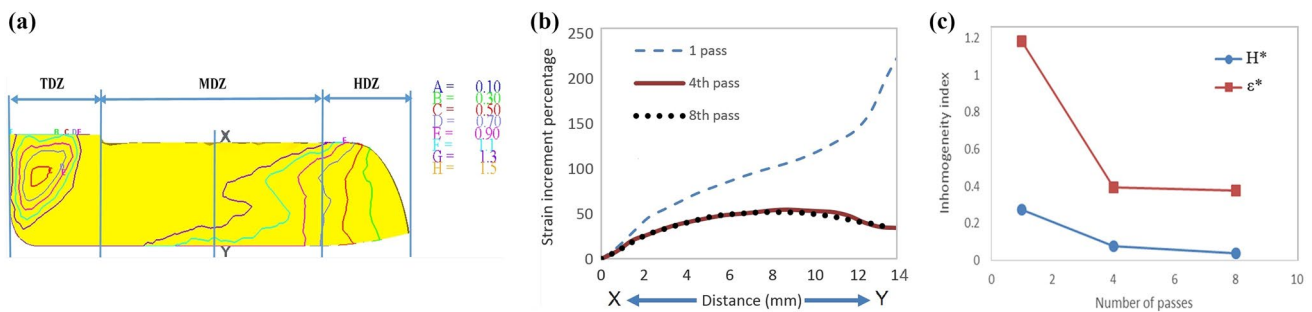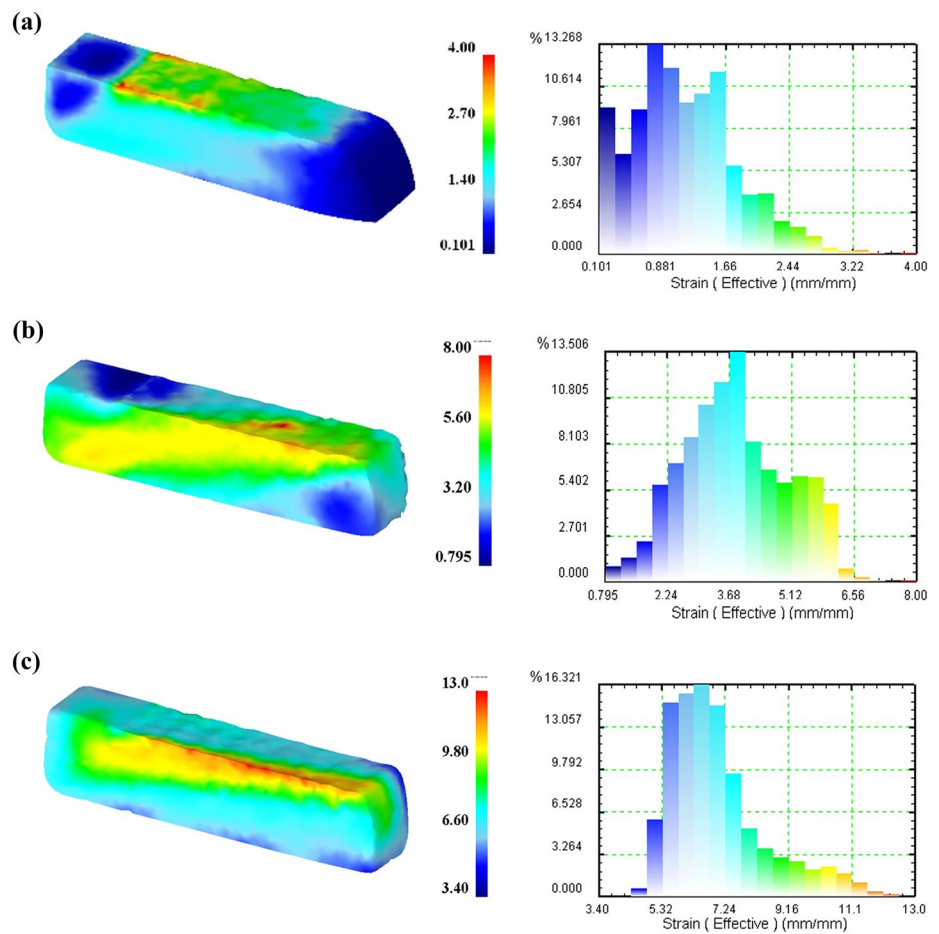
Fig. 11 a Effective plastic strain contour across longitudinal direction after one pass ECAE process, **b** strain increment percentage through thickness direction and **c** effect of ECAE pass number on inhomogeneity index

a constant, d is the mean (sub) grain size, θ_{LAB} the mean misorientation of LAGBs, f the fraction of HAGBs and k the Hall–Petch constant. Using the values of G = 45.6GPa, ν = 0.324, h = 0.203 nm, b = 0.256 nm, M = 3.06, α = 0.24, k = 0.14Mpa $\sqrt{m}$ for copper, and inserting the microstructural factors via the EBSD characterization (which is averaged through the billet thickness), the yield strength was calculated.

Although the experimental strengths confirm the theoretical predictions at first passes, steady trend in the determined yield strength up to eight passes can be observed. The discrepancy may be affected by three essential issues. First, the strengthening due to texture evolution considered constant in Eq. (4) [33]. Second, the specific angle of the boundaries at which their strengthening roles transform is designated as 15° [34]. Third, boundaries with a misorientation above 2° are merely accommodated in the analyses,
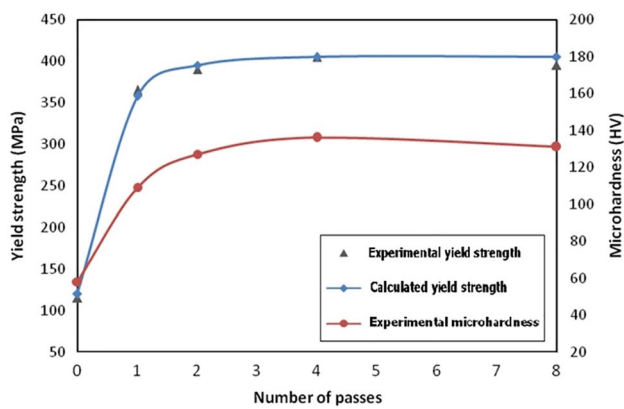
Fig. 12 The dependence of calculated and measured yield strength as well as the mean microhardness on the number of passes

while by increasing the pass numbers, a fraction of very LAGBs still exists in the microstructure. Resembling the tensile results, the hardness enhancement after the first pass is notable as a result of drastic increase in dislocation density and the onset of smaller (sub) grain production. Between two and four passes, the increasing rate of hardness and yield strength is low and it reaches its maximum with more than four passes. From the four to the eight passes, a moderate decrease is discerned in the measurements. Indeed, the strain softening arise on the basis of dislocation rearrangement [35]. Therefore, the dislocation density growth likely reduces due to annihilation and formation of locks or dipoles [36]. It is evidently shown that the microhardness is correlated with yield strength, by the ratio in the range 3.02–3.29 for the case of Hv $\approx \sigma_y/3$ as has been earlier presented [37].

5 Conclusions

In the recent study, C11000 billets were ECA-extruded up to 8 passes. Then, the microhardness, yield strength, subgrain size, area fraction of the HAGBs, misorientation angles and the texture of the copper were assessed. According to the results, the microstructure and microhardness of the specimens was heterogeneous up to 4 passes, whereas thickness gradients nearly disappeared after eighth pass. The simulation analysis of the plastic strain represented a trend similar to that of experimental data distribution. The ECAE process increased the hardness and strength of the copper up to four passes. Then, they got decreased during the further passes, whereas the increment in the calculated yield strength was constant. This phenomenon was attributed to take a stable texture and constant critical angle of the boundaries plus the ignoring boundaries with a misorientation angle below 2°.

References

1. Ma M, Li Z, Qiu W, Xiao Z, Zhao Z and Jiang Y, *J Alloys Compd* **788** (2019) 50.
2. Mousavi S E, Sonboli A, Meratian M, Amirnejad M, Mohamadi Azghandi S H and Munroe P, *Mater Sci Eng A* **802** (2021) 140654.
3. Alawadhi M Y, Sabbaghianrad S, Huang Y and Langdon T G, *Mater Sci Eng A* **802** (2021) 140546.
4. Frint S, Hockauf M, Frint P and Wagner M. F.-X., *Mater Des* **97** (2016) 502.
5. Valiev R Z and Langdon T G, *Prog Mater Sci* **51** (2006) 881.
6. Abd El Aal M I, Um H Y, Yoon E Y and Kim H S, *Mater Sci Eng A* **625** (2015) 252.
7. Gu Y, Ma A, Jiang J, Yuan Y and Wu H, *Mater Charact* **168** (2020) 110513.
8. Iwahashi Y, Wang J, Horita Z, Nemoto M and Langdon T G, *Scripta Mater* **35** (1996) 143.
9. Kim H S, Seo M H and Hong S I, *Mater Sci Eng A* **291** (2000) 86.
10. Terhune S D, Swisher D L, Oh-Ishi K, Horita Z, Langdon T G and Mcnelley T R, *Metall Mater Trans A* **33** (2002) 2173.
11. Necker C T, Alexander D J and Beyerlein I J, *Mater Sci Forum* **495–497** (2005) 857.
12. Wongsa-Ngam J, Kawasaki M and Langdon T G, *Mater Sci Eng A* **556** (2012) 526.
13. Ma M, Li Z, Qiu W, Xiao Z, Zhao Z, Jiang Y, Xia Z and Huang H, *J Alloys Compd* **820** (2020) 153112.
14. Basavaraj V P, Chakkingal U and Kumar T S P, *J Mater Process Technol* **209** (2009) 89.
15. Yang X, Wang D, Wu Z, Yi J, Ni S, Du Y and Song M, *Mater Sci Eng A* **658** (2016) 16.
16. Segal V M, *Mater Sci Eng A* **338** (2002) 331.
17. Kim W J, Namgung J C and Kim J K, *Scripta Mater* **53** (2005) 293.
18. Li S, Beyerlein I J and Necker C T, *Acta Mater* **54** (2006) 1397.
19. Beyerlein I J and Toth L S, *Prog Mater Sci* **54** (2009) 427.
20. Skrotzki W, Scheerbaum N, Oertel C G, Brokmeier H G, Suwas S and Toth L S, *Mater Sci Forum* **503-504** (2006) 99.
21. Hull D, Bacon D J *Introduction to Dislocations*. Elsevier: New Jersey (2011) p 43
22. Reihanian M, Ebrahimi R, Moshksar M M, Terada D and Tsuji N, *Mater Charact* **59** (2008) 1312.
23. An X H, Lin Q Y, Wu S D and Zhang Z F, *Mater Sci Eng A* **527** (2010) 4510.
24. Duan Y L, Xu G F, Tang L, Li Z and Yang G, *Mater Sci Eng A* **648** (2015) 252.
25. Huang X, Tsuji N, Hansen N and Minamino Y, *Mater Sci Eng A* **340** (2003) 265.
26. Humphreys J and Hatherly M, *Recrystallization and Related Annealing Phenomena*, Oxford, Elsevier (2004).
27. Hansen N, Mehl R F and Medalist A, *Metall Mater Trans A* **32** (2001) 2917.
28. Ghosh A and Ghosh M, *Mater Today Commun* **26** (2021) 102112
29. Hansen N and Jensen D J, *Philos Trans R Soc Lond A* **357** (1999) 1447.
30. Hughes D A, *Mater Sci Eng A* **319–321** (2001) 46
31. Hansen N, *Scripta Mater* **51** (2004) 801.
32. Wang J N, *Mater Sci Eng A* **206** (1996) 259.
33. Lapovok R, Dalla Torre F H, Sandlin J, Davies C H J and Estrin Y, *J Mech Phys Solids* 53 (2005) 729.
34. Kamikawa N, Huang X, Tsuji N, Hansen N and Minamino Y, *Mater Sci Forum* **512** (2006) 91.
35. Hansen N, Huang X and Hughes D A, *Mater Sci Eng A* **317** (2001) 3..

36. Goerdeler M and Gottstein G, *Mater Sci Eng A* **309–310** (2001) 377

37. Lianxi H, Yuping L, Erde W and Yang Y, *Mater Sci Eng A* **422** (2006) 327..